Supporting Information. *Elucidation of amyloid β-protein oligomerization mechanisms: Discrete Molecular Dynamics Study*

B. Urbanc[1]*, M. Betnel[2], L. Cruz[1], G. Bitan[3,4], and D. B. Teplow[3,4]

[1]*Department of Physics, Drexel University, Philadelphia, PA 19104, USA;* [2]*Department of Physics, Boston University, Boston, MA 02215;* [3]*Department of Neurology, David Geffen School of Medicine, University of California, Los Angeles, CA 90095-7334, USA;* [4]*Molecular Biology Institute and Brain Research Institute, University of California, Los Angeles, CA 90095-7334, USA.*

Time Evolution of Oligomer Size Distributions

Initially, each DMD simulation trajectory consisted of 32 spatially–separated peptides in random-coil–like conformations. Thus, the probability distributions of oligomer sizes for all four peptides (Aβ_{1-40}, Aβ_{1-42}, [E22G]Aβ_{1-40}, and [E22G]Aβ_{1-42}) at the simulation time $t = 0$ were equivalent and characterized by a probability $P(n) = 1$ at the oligomer size n=1 (and $P(n) = 0$ for all $n > 1$). Figs. S1a-d show probability distributions, $P(n)$, for each of the four peptides at 4 different time windows: (1) 9-10 $\times$ 10^6, (2) 19-20 $\times$ 10^6, (3) 29-30 $\times$ 10^6, and (4) 39-40 $\times$ 10^6 simulation time steps. Within each time window, we selected frames that were as independent of each other as possible, to avoid biasing the calculation of the standard error of the mean (SEM) for each oligomer size. Within each time window, 3 time frames (e.g., at 9, 9.5, and 10 $\times$ 10^6 time steps) were thus selected for each of the 8 trajectories—in total 24 different populations of oligomers for each of the

*Corresponding Author: brigita@drexel.edu

four peptides to calculate the four oligomer size distribution probabilities $P(n)$. The results demonstrate how the characteristic peaks in $P(n)$ change with simulation time on a 10×10^6 time scale. These results show that the main characteristics of the probability distributions already develop within the first 10×10^6 time steps. However, the distributions keep evolving with time. Of the four peptides, only Aβ_{1-40} was characterized by a probability distribution that remained the same on a long time scale, between 20 and 40×10^6 time steps (Figure S1a). Aβ_{1-42} oligomers with a characteristic size 5-6 were already present at 10×10^6 time steps. However, larger oligomers with sizes $\sim$12 appeared at 20×10^6 time steps and became more abundant between 20 and 40×10^6 time steps, at the expense of Aβ_{1-42} hexamers (Figure S1b). The characteristic peak at oligomer sizes 5-6 in the [E22G]Aβ_{1-40} distribution appeared at 20×10^6 time steps and became more pronounced between 20 and 40×10^6 time steps (Figure S1c). Interestingly, the [E22G]Aβ_{1-42} distribution did not show very significant changes after 10×10^6 time steps (Figure S1d). However, because the relative number of Aβ_{1-42} hexamers (Figure S1b) decreased between 30 and 40 $\times 10^6$ time steps, the relative numbers of Aβ_{1-42} and [E22G]Aβ_{1-42} hexamers were similar at these longer time scales, which is a result consistent with PICUP observations.[1]

Based on finite time-scale simulations, we cannot conclude whether any of four probability distributions reached a true steady state. However, we explored whether the distributions changed significantly on time scales of 1×10^6, 2×10^6, and 5×10^6 simulation time steps by applying the chi–square test that compared two subsequent distributions and gave the p-value, i.e. the probability that the two distributions were statistically equivalent. For each of the four peptides, we first calculated histograms of oligomer sizes using a sliding time window: 1-2 $\times 10^6$, 2-3 $\times 10^6 \ldots$, 39-40 $\times 10^6$ time steps. Within each of the sliding time windows, we selected populations of monomers and oligomers of all 8 trajectories at 3 time frames, e.g., at 1, 1.5, and 2×10^6, to calculate the histograms of oligomer sizes for each of the four peptides. We then calculated the p-values of two subsequent histograms of oligomer sizes of the *same* peptide, which were separated by time lags, Δt, of 1, 2, and 5×10^6 time steps. The time evolution of the p-values is presented in Fig. S2 for each of the four peptides at the three different values of Δt. The distribu-

tions were changing significantly (p-value < 0.05) within $\Delta t = 1 \times 10^6$ only within the first 5×10^6 time steps (Figure S2a). A similar conclusion can be made for changes within $\Delta t = 2 \times 10^6$ (Figure S2b), even though the p-value fluctuations were larger than in Figure S2a. However, the changes within $\Delta t = 5 \times 10^6$ (Figure S2c) were significant within the first 10-15 $\times 10^6$ time steps and were different for each of the four different peptides. The steady state of the probability distribution on time scales of $\Delta t = 5 \times 10^6$ (Figure S2c) was first reached by [E22G]Aβ_{1-42} (at 5-10 $\times 10^6$), followed by Aβ_{1-40} (at $\sim$10 $\times 10^6$), while Aβ_{1-42} and [E22G]Aβ_{1-40} needed the longest time to reach the steady state (at 15-20 $\times 10^6$), consistent with observations in Figure S1. The p-values in Figure S2c also showed the largest fluctuations, consistent with the largest time lag of $\Delta t = 5 \times 10^6$. Interestingly, on a time scale 20-40 $\times 10^6$, the two Arctic peptides displayed the largest fluctuations in p-values ([E22G]Aβ_{1-40} even more so than [E22G]Aβ_{1-42}), most likely indicating an onset of assembly into larger structures, also consistent with emergence of small peaks at oligomer sizes ≥ 13 in Figure S1, corresponding to elongated protofibril-like oligomers.

Because the time evolution of the probability distributions in Figure S1 showed some temporal changes between 20 and 40 $\times 10^6$ time steps, we next asked whether the probability distributions calculated within the time window 19-20 $\times 10^6$ significantly differed from those calculated within the time window 39-40 $\times 10^6$. The p-values of the corresponding chi–square test (along the diagonal elements of Table S1) demonstrated that: (1) the Aβ_{1-40} distribution did not change significantly (p-value > 0.05); (2) the changes in the Aβ_{1-42} and [E22G]Aβ_{1-42} distributions were on the border of significance (0.01 < p-value < 0.05) and (3) [E22G]Aβ_{1-40} distribution changed significantly (p-value = 0.0089). Despite these changes, the overall characteristics of distributions belonging to the four peptides did not change. For example, [E22G]Aβ_{1-40} distribution, which was the only one that changed significantly, showed at later times a smaller relative numbers of dimers and trimers and a larger relative number of hexamers. Thus, the relative number of [E22G]Aβ_{1-40} paranuclei, which was comparable to the relative number of Aβ_{1-42} paranuclei within the time window 19-20 $\times 10^6$, increased and surpassed the relative number of Aβ_{1-42} paranuclei within the time window 39-40 $\times 10^6$ (Figure S1). We also examined the temporal changes in individual

distributions by quantifying the distribution differences among the four peptides at a fixed time window. The results of this cross-comparison are reported in Table S1 for each of the two time windows: 19-20 $\times$ 10^6 (the p-values below the diagonal) and 39-40 $\times$ 10^6 (the p-values above the diagonal). These off-diagonal p-values were one or more orders of magnitude smaller than the p-values along the diagonal, demonstrating that the distribution differences among the four *different* peptides were significantly larger that the time–induced distribution differences of the *same* peptide.

β-Strand Propensity Per Residue

Our results showed that the β-strand secondary structure was the most prominent secondary structure in oligomers of all four peptides under study. Different peptide regions were shown to have distinct propensities to form the β-strand structure (Figure 6), depending both on the specific peptide as well as the oligomer order. To elucidate these differences in detail, we systematically compared the β-strand propensity per residue for Aβ_{1-40}, Aβ_{1-42}, [E22G]Aβ_{1-40}, and [E22G]Aβ_{1-42} dimers and hexamers, by plotting all 28 pairs of β-strand propensity versus residue curves (Figure S4). The graphs in Figure S4 are arranged such that the first three rows include 6 graphs corresponding to data of all possible dimer pairs. Analogously, the last three columns include 6 graphs corresponding to data of all possible hexamer pairs. The remaining 16 graphs (a square matrix of 16 graphs comprising the last 4 rows and the first 4 columns) contain data of dimers-hexamers pairs of the four peptides.

Dimer-Dimer Pairs. Comparing the data of all dimer pairs (the first 3 rows of graphs in Figure S4), Aβ_{1-40} and Aβ_{1-42} dimers showed overall the largest differences in the β-strand propensities per residue curves ($P(2,1)$). Aβ_{1-40} and Aβ_{1-42} β-strand propensities differed at the N-terminal region A2-F4, where Aβ_{1-40} but not Aβ_{1-42} showed β-strand propensity of up to 0.3 ($P(2,1)$). Of all dimers, only Aβ_{1-40} dimers were characterized by the β-strand propensity at A2-F4. In contrast, Aβ_{1-42} dimers showed a significantly higher β-strand propensity at R5-H6, G9-E11, L17-A21, and V39-I41 ($P(2,1)$). Significant β-strand propensities at R5-H6 and G9-V11 were observed

in all but Aβ_{1-40} dimers. [E22G]Aβ_{1-40} dimers showed increased β-strand propensities at F19-V24 of similar values to those in Aβ_{1-42} dimers at the CHC (L17-A21). β-Strand propensities at the CTR (V39-I41) were non-zero in Aβ_{1-42} and [E22G]Aβ_{1-42} dimers but were zero in Aβ_{1-40} and [E22G]Aβ_{1-40} dimers. Except for this difference at the CTR, [E22G]Aβ_{1-40} and Aβ_{1-42} dimers were characterized with the most similar β-strand propensities ($P(3,2)$). [E22G]Aβ_{1-42} and Aβ_{1-42} propensities were also quite similar except at R5-H6, H13-H14, and L17-A21, where [E22G]Aβ_{1-42} dimers showed significantly lower propensities than Aβ_{1-42} dimers ($P(4,2)$). Similarly, [E22G]Aβ_{1-42} dimers showed lower propensities than [E22G]Aβ_{1-40} dimers at R5-H6, Y10-V24, and N27-G29 but showed higher propensities at M35 and the CTR ($P(4,3)$).

Hexamer-Hexamer Pairs. Comparing the data of all hexamer pairs (the last 3 columns of graphs in Figure S4), β-strand propensities among pairs of the 4 peptides displayed similar tendencies as in dimers. Only Aβ_{1-40} hexamers were characterized by high β-strand propensities (0.4-0.6) at A2-F4. Aβ_{1-42} hexamers were characterized by higher β-strand propensities than Aβ_{1-40} hexamers at R5-E11, H13-F20, G25-S26, G29-I31, L34, and at the CTR ($P(6,5)$). Only Aβ_{1-42} and [E22G]Aβ_{1-42} hexamers had a non-zero propensity (0.2-0.3) at the CTR. The two most distinct features between the β-strand propensity curves were between Aβ_{1-40} and the two Arctic peptides, [E22G]Aβ_{1-40} ($P(7,5)$) and [E22G]Aβ_{1-42} ($P(8,5)$). Hexamers of both Arctic peptides were characterized by significantly higher β-strand propensities along the entire peptide sequence relative to hexamers of the wild-type peptides (except at A2-F4). The two most similar β-strand propensity curves were those belonging to Aβ_{1-42} and [E22G]Aβ_{1-42} hexamers ($P(8,6)$), where [E22G]Aβ_{1-42} had slightly higher β-strand propensities at R5-H6, E11-Q15, L17-F19, S26-K28, and M35-V36. The β-strand propensities of Aβ_{1-42} and [E22G]Aβ_{1-40} hexamers ($P(7,6)$) were more distinct than in dimers: [E22G]Aβ_{1-40} hexamers had higher β-strand propensities at R5-H6, Y10-H13, F20-V24, and N27-I31 but none at the CTR (in contrast to Aβ_{1-42} hexamers). [E22G]Aβ_{1-40} hexamers had higher propensities at G9-H13, A21-G25, N27, and A30-I31 relative to [E22G]Aβ_{1-42} hexamers, which were characterized by higher propensities at L17-F19, M35-V36, and at the CTR ($P(8,7)$).

Dimer-Hexamer Pairs. We finally compared pairs of β-strand versus residue curves of dimers and hexamers, including all 4 peptides (the last 4 rows and the first 4 columns of graphs in Figure S4). Each of the 4 diagonal graphs, $P(5,1)$, $P(6,2)$, $P(7,3)$, and $P(8,4)$, contained the β-strand propensities of dimers and hexamers of the same peptide. These diagonal graphs thus elucidated the differences in β-strand propensities due to different oligomer order. In Aβ_{1-40}, the β-strand propensities at A2-F4 increased substantially from $\sim$0.3 in dimers to $\sim$0.55 in hexamers ($P(5,1)$). In the rest of the sequence (except at A2-F4), β-strand propensities were decreased in hexamers relative to dimers ($P(5,1)$). This decrease of the overall β-strand propensity in hexamers relative to dimers was characteristic also of Aβ_{1-42} ($P(6,2)$). In [E22G]Aβ_{1-40}, however, the changes in the β-strand propensity induced by higher oligomer order (dimers to hexamers) were minimal ($P(7,3)$). Interestingly, in [E22G]Aβ_{1-42} a different tendency was observed: while β-strand propensities remained unchanged at the C-terminal region I31-A42, the values at R5-H6, H13-F20, N27-G29 were *increased* in hexamers relative to dimers ($P(8,4)$).

β-Strand propensities in Aβ_{1-40} dimers were compared to those of hexamers of Aβ_{1-42} ($P(6,1)$), [E22G]Aβ_{1-40} ($P(7,1)$), and [E22G]Aβ_{1-42} ($P(8,1)$). The overall β-strand propensities in Aβ_{1-42} hexamers were similar to those in Aβ_{1-40} dimers, where Aβ_{1-40} dimers showed higher propensities at A2-F4, V12-H14, and L34-V36 and Aβ_{1-42} hexamers displayed higher propensities at R5-E11, G25-S26, and the CTR ($P(6,1)$). Similar tendencies were observed when Aβ_{1-40} dimers were compared to [E22G]Aβ_{1-40} hexamers: [E22G]Aβ_{1-40} hexamers had higher propensities at R5-V12 and A21-I31 ($P(7,1)$). [E22G]Aβ_{1-42} had higher propensities at R5-E11, H14-F19, S26-G29, and M35-V40 compared to Aβ_{1-40} dimers ($P(8,1)$).

We compared β-strand propensities in Aβ_{1-42} dimers to those of hexamers of Aβ_{1-40} ($P(5,2)$), [E22G]Aβ_{1-40} ($P(7,2)$), and [E22G]Aβ_{1-42} ($P(8,2)$). The largest differences between the β-strand versus residue curves were observed between Aβ_{1-42} dimers and Aβ_{1-40} hexamers, where the former were characterized by significantly higher propensities at H5-H14, V18-F20, A30-I31, L34-G37, and the CTR than the latter ($P(5,2)$). Overall amounts of the β-strand propensity were comparable between Aβ_{1-42} dimers and [E22G]Aβ_{1-40}/[E22G]Aβ_{1-42} hexamers (($P(7,2)$ and

($P(8,2)$).

β-Strand propensities in [E22G]Aβ_{1-40} dimers were then compared to those of hexamers of Aβ_{1-40} ($P(5,3)$), Aβ_{1-42} ($P(6,3)$), and [E22G]Aβ_{1-42} ($P(8,3)$). As expected, the largest differences were observed between [E22G]Aβ_{1-40} dimers and Aβ_{1-40} hexamers, which were characterized by a decreased propensities along most of the peptide (except at A2-F4), at R5-Q15 and L17-G37 ($P(5,3)$). The propensities of [E22G]Aβ_{1-40} dimers and Aβ_{1-42} hexamers were following similar trends as [E22G]Aβ_{1-40} dimers showing consistently increased propensities at Y10-H14, F19-V24, and N27-G37 compared to Aβ_{1-42} hexamers ($P(6,3)$). [E22G]Aβ_{1-40} dimers and [E22G]Aβ_{1-42} hexamers had comparable β-strand propensities with some variations along the sequence: [E22G]Aβ_{1-42} hexamers had decreased propensities at Y10-E11, F20-V24, and A30-L34 as well as increased propensities at R5-H6, H13-F19, M35-V36, and the CTR relative to [E22G]Aβ_{1-40} dimers ($P(8,3)$).

Further, we compared β-strand propensities of [E22G]Aβ_{1-42} dimers and hexamers of Aβ_{1-40} ($P(5,4)$), Aβ_{1-42} ($P(6,4)$), and [E22G]Aβ_{1-40} ($P(7,4)$). [E22G]Aβ_{1-42} dimers showed increased propensities at R5-V12, L17-F19, G25-S26, A30-I31, L34-V36, and the CTR as well as decreased propensities at A2-F4 ($P(5,4)$). β-Strand propensities of [E22G]Aβ_{1-42} dimers and Aβ_{1-42} hexamers were quite similar: Aβ_{1-42} hexamers showed higher propensities at R5-H6, Q15-V18, and G25-K28 as well as lower propensities at A30-I31 and L34-V36 relative to [E22G]Aβ_{1-42} dimers ($P(6,4)$). [E22G]Aβ_{1-40} hexamers had *higher* propensities at the N-terminal two-thirds of the sequence at R5-H6, G9-H13, K16-L17, F20-V24, and N27-I31 as well as *lower* propensities at G33-V36 and the CTR ($P(7,4)$)

Tertiary and quaternary structures of Aβ oligomers

To systematically examine the contact maps, we defined several regions enclosed in boxes on (a) intramolecular and (b) intermolecular contact maps with a high density of contacts. On each intramolecular (Figures S6a-h) and intermolecular (Figures S7a-h) contact map, we depicted 4 boxes marked by numbers (1-4). In the following we describe the differences between these maps,

referring to these boxes by their numbers. Note that the boxes were defined for each of the two Figures S6 and S7 and box definitions were valid only within each of the figures separately.

Tertiary structures. Tertiary structures of dimers and hexamers for all four peptides are depicted in Figures S6a-h. When compared among dimers and hexamers of all 4 peptides, these structures had some basic common features. They were rather similar to folded structures of the four individual peptides.[2] This result suggests that oligomer formation may not be accompanied by major structural changes of individual peptides. In oligomers of all four peptides, the region with the largest density of intramolecular contacts was the central folding region, which included contacts between the CHC and MHR (Figures S6a-h, Box 4, lower left triangle). Similarly, intramolecular contacts at the CTR with the strongest contact V36–V39 were observed in all oligomers under study (Figures S6a-h, Box 3, lower left triangle). As expected, the intramolecular contacts around V36–V39 contact were strongest and more numerous in oligomers of Aβ_{1-42} and [E22G]Aβ_{1-42}. The N-terminal E2–F4 region was involved, to different degrees, in intramolecular contacts with the CHC, MHR, and CTR in all 4 peptides (Figures S6a-h, Box 2, lower left triangle). These contacts varied among the four peptides and between dimers and hexamers of the same peptide.

Intramolecular contact maps of Aβ_{1-40} dimers and hexamers (Figures S6a and e) were indistinguishable from each other, demonstrating that tertiary structures of Aβ_{1-40} dimers and hexamers were identical. Box 1 includes all intramolecular contacts within the CHC (lower left triangle) as well as the hydrogen bond propensities (upper right triangle). Among dimers and hexamers of all 4 peptides, Aβ_{1-40} dimers and hexamers were the only oligomers characterized by an off–diagonal hydrogen bonding pattern indicating non-zero α-helix propensity in the CHC.

A hydrogen bonding pattern indicating non-zero α-helix propensity was observed in the region G25-G33, which contains 3 glycines in a GXXXGXXXG motif, of all oligomers of all 4 peptides (Figures S6a-h, Box 4, upper right triangle) and was stronger and comprised a wider region (G22-G33) in oligomers of the Arctic peptides (Figures S6c-d and g-h, Box 4, upper right triangle) with the GXXGXXXGXXXG motifs.

Aβ_{1-42} dimers were characterized by the strongest (Figure S6b, Box 1, lower left triangle) and

Aβ_{1-42} hexamers by the weakest (Figure S6b, Box 1, lower left triangle) intramolecular contacts in the CHC. This result showed that Aβ_{1-42} oligomerization from dimers to hexamers was accompanied by a partial loss of intramolecular contacts within the CHC. No such loss of contacts in the CHC upon oligomer formation from dimers to hexamers was observed for the other three peptides. Contacts of A2–F4 with the CHC, MHR, and CTR were stronger and more numerous in Aβ_{1-42} dimers than in Aβ_{1-42} hexamers (Figures S6b and f, Box 2, lower left triangle). The intramolecular contacts involving the MHR and CTR (Figures S6b and f, Box 3, lower left triangle) were somewhat *stronger* in Aβ_{1-42} hexamers than in Aβ_{1-42} dimers, possibly due to a significantly higher hydrogen bond propensity V36–V39 (Figure S6f, Box 3, upper right triangle), which might stabilize the tertiary structure at the CTR. This region was the only one that showed increased intramolecular contacts in Aβ_{1-42} hexamers relative to Aβ_{1-42} dimers. Among oligomers of all 4 peptides under study, Aβ_{1-42} oligomers were characterized by the least strong intramolecular contacts within the central folding region, which included contacts between the CHC and MHR (Figures S6a-h, Box 4, lower left triangle). Interestingly, Aβ_{1-42} dimers had somewhat lower hydrogen bond propensities in this region than Aβ_{1-42} hexamers (Figures S6b and f, Box 4, upper right triangle). This result suggests that partial destabilization of intramolecular contacts within the central folding region might promote Aβ_{1-42} hexamer formation.

[E22G]Aβ_{1-40} hexamers had somewhat weaker contacts in the central folding region relative to [E22G]Aβ_{1-40} dimers (Figures S6c and g, Box 4, lower left triangle), even though these contacts were stronger than in Aβ_{1-42} hexamers (Figures S6f, Box 4, lower left triangle). The hydrogen bond pattern in [E22G]Aβ_{1-40} dimers, which indicated a β-hairpin structure (Figures S6c, Box 4, upper right triangle), was not present in [E22G]Aβ_{1-40} hexamers (Figures S6g, Box 4, upper right triangle). As in Aβ_{1-42}, this observation was consistent with a hypothesis that partial destabilization of intramolecular contacts within the central folding region is needed to form [E22G]Aβ_{1-40} hexamers. Consistent with this hypothesis was also the observation that the intramolecular contacts in [E22G]Aβ_{1-42} hexamers, which formed with lower probability just like Aβ_{1-40} hexamers, were almost the same as in [E22G]Aβ_{1-42} dimers (Figures S6d and h). Instead of destabilizing the

contacts in the central folding region upon hexamer formation (a feature characteristic in particular of Aβ_{1-42} hexamers), these contacts were somewhat *stronger* in [E22G]Aβ_{1-42} hexamers than in [E22G]Aβ_{1-42} dimers (Figures S6d and h, Box 4, lower left triangle) and the hydrogen bonding propensities were somewhat increased as well (Figures S6d and h, Box 4, upper right triangle). In contrast, a relatively high hydrogen bond propensity at V36–V39 that was characteristic for Aβ_{1-42} hexamers was present in [E22G]Aβ_{1-42} dimers (Figure S6d, Box 3, upper right triangle). These results combined suggest that (i) stabilization of the CTR-MHR intramolecular contacts through formation of the hydrogen bond V36–V39 and (ii) destabilization of intramolecular contacts in the central folding region might be two key factors associated with oligomer formation.

Quaternary structures. Quaternary structures of dimers and hexamers for all four peptides are depicted in Figures S7a-h. These structures when compared among dimers and hexamers of all 4 peptides had some common basic features. We observed an overall increase in intermolecular contact strengths between dimers (Figures S7a-d) and hexamers (Figures S7e-h). This was a consequence of the fact that in a hexamer, where a peptide was in contact with five other equivalent peptides, the number of possible contacts between any two residues that belong to different peptides would be larger than in a dimer. Basic quaternary structure differences between Aβ_{1-40} and Aβ_{1-42} oligomers of order 5 (or higher) were described in prior work[3,4] that demonstrated that Aβ_{1-40} oligomer formation was driven by intermolecular interactions between the CHC region, while Aβ_{1-42} oligomerization was dominated by intermolecular interactions of CTRs with CTR, MHR, and CHC regions of other peptides within an oligomer.

The intermolecular contact maps of Aβ_{1-40}, Aβ_{1-42}, [E22G]Aβ_{1-40}, and [E22G]Aβ_{1-42} dimers (Figures S7a-d) were relatively similar to each other, suggesting that dimer formation was similar in all four peptides. Here we compared mostly the quaternary structures of Aβ_{1-40}, Aβ_{1-42}, [E22G]Aβ_{1-40}, and [E22G]Aβ_{1-42} hexamers, which showed some distinct features (Figures S7e-h). The region A2–F4 was highly involved in hexamer formation in only Aβ_{1-40} (Figures S7e-h, Box 1, lower left triangle) consistent with our data on β-strand propensity (Figures S4). Analysis of the hydrogen bonding propensities showed a pattern consistent with parallel intermolecular

β-strands at A2–F4 (Figure S7e, Box 1, upper right triangle). As shown previously,[3,4] Aβ_{1-40} oligomer formation was dominated by interactions among the CHC regions, between the CHC and MHR regions, and between the CHC and CTR regions (Figure S7e, Boxes 3 and 4, lower left triangle). These contacts were present also in intermolecular contact maps of Aβ_{1-42}, [E22G]Aβ_{1-40}, and [E22G]Aβ_{1-42} hexamers, but were mostly weaker, in particular in Aβ_{1-42} hexamers (Figures S7f-h, Boxes 3 and 4, lower left triangle). In Aβ_{1-42} hexamers, the strongest contacts were formed among the CTR regions, between the CTR and MHR regions, and between CTR and CHC regions (Figure S7f, Boxes 4 and 5, lower left triangle). Intermolecular contacts between A2–F4 and CHC, MHR, and CTR were present in Aβ_{1-42}, [E22G]Aβ_{1-40}, and [E22G]Aβ_{1-42} hexamers but were significantly weaker than in Aβ_{1-40} hexamers (Figures S7e-h, Box 2, lower left triangle). On the other hand, the peptide region A30-V40 (A30-A42) was characterized by significantly larger number of intermolecular contacts in Aβ_{1-42}, [E22G]Aβ_{1-40}, and [E22G]Aβ_{1-42} hexamers relative to Aβ_{1-40} hexamers. These contacts were strongest in Aβ_{1-42} hexamers. Intermolecular contact maps of [E22G]Aβ_{1-40}, and [E22G]Aβ_{1-42} hexamers were more similar to the contact maps of Aβ_{1-42} hexamers but showed more intermolecular contacts among CHC regions than Aβ_{1-42} hexamers, suggesting that the quaternary structure of the Arctic peptides had most features of Aβ_{1-42} hexamers but also some characteristics of Aβ_{1-40} hexamers.

Table 1: *The chi–square test results for the probability that two histograms of oligomer size are equal. The p-values result from a comparison between the histograms of oligomer size of the same peptide obtained by averaging over time frames at (i) 19, 19.5, and 20 $\times$ 10^6 steps and (ii) 39, 39.5, and 40 $\times$ 10^6 steps. The p-values below the diagonal p-values in the table are a result of comparisons between the histograms of oligomer size of two different peptides obtained by averaging over time frames at 19, 19.5, and 20 $\times$ 10^6 steps. The p-values above the diagonal p-values in the table are a result of comparisons between the histograms of oligomer size of two different peptides obtained by averaging over time frames at 39, 39.5, and 40 $\times$ 10^6 steps.*

p-values	Aβ_{1-40}	Aβ_{1-42}	[E22G]Aβ_{1-40}	[E22G]Aβ_{1-42}
Aβ_{1-40}	1.3×10^{-1}	1.5×10^{-12}	7.6×10^{-9}	2.1×10^{-9}
Aβ_{1-42}	6.6×10^{-11}	2.2×10^{-2}	2.2×10^{-4}	1.1×10^{-9}
[E22G]Aβ_{1-40}	7.4×10^{-7}	1.4×10^{-3}	8.9×10^{-3}	1.1×10^{-4}
[E22G]Aβ_{1-42}	5.1×10^{-10}	3.9×10^{-7}	4.6×10^{-6}	2.4×10^{-2}

FIGURE CAPTIONS

Fig. S1: Time evolution of probability distributions of oligomer sizes for (a) Aβ_{1-40}, (b) Aβ_{1-42}, (c) [E22G]Aβ_{1-40}, and (d) [E22G]Aβ_{1-42}. The scale on the x-axis was adjusted to the probability distribution of each peptide to best display the differences among the curves obtained at 4 different time windows: $t = 9-10\times10^6$ (black solid lines), $t = 19-20\times10^6$ (red solid lines), $t = 29-30\times10^6$ (black dashed lines), and $t = 39-40\times10^6$ (red dashed lines). The error bars correspond to SEM.

Fig. S2: Time progression of the p-values obtained by applying the chi–square test to quantify whether two histograms of oligomer sizes that were obtained at two different time windows, Δt apart, were statistically equivalent for (a) $\Delta t = 1\times10^6$, (b) $\Delta t = 2\times10^6$, and (c) $\Delta t = 5\times10^6$. The p-values were calculated for each peptide Aβ_{1-40} (solid black lines), Aβ_{1-42} (solid red lines), [E22G]Aβ_{1-40} (dashed black lines), and [E22G]Aβ_{1-42} (dashed red lines), separately.

Fig. S3: Solvent accessible surface area (SASA) per residue for (a) Aβ_{1-40} and (b) Aβ_{1-42} dimers at $E_{CH} = 0$, $E_{CH} = 10^{-6}$, and $E_{CH} = 10^{-2}$. The error bars correspond to SEM.

Fig. S4: Pair plots of $\langle\beta$-strand$\rangle$ per residue for dimers and hexamers of all four peptides: Aβ_{1-40}, Aβ_{1-42}, [E22G]Aβ_{1-40}, and [E22G]Aβ_{1-42}. The error bars correspond to SEM. The solid curves correspond to the wild-type peptides and the dotted curves correspond to the Arctic peptides. The curves for the shorter peptides, Aβ_{1-40} and [E22G]Aβ_{1-40}, are plotted in black and the curves for Aβ_{1-42} and [E22G]Aβ_{1-42} are plotted in red. Circles (open for Aβ_{1-40} and [E22G]Aβ_{1-40} and filled for Aβ_{1-42} and [E22G]Aβ_{1-42} correspond to dimers while squares (crossed for Aβ_{1-40} and [E22G]Aβ_{1-40} and filled for Aβ_{1-42} and [E22G]Aβ_{1-42} correspond to hexamers. Labels on the y-axes, P(i,j), are β-strand propensities (with values $\in [0,1]$) for oligomer types i and j, where the types are defined by: 1-Aβ_{1-40} dimers, 2-Aβ_{1-42} dimers, 3-[E22G]Aβ_{1-40} dimers, 4-[E22G]Aβ_{1-42} dimers, 5-Aβ_{1-40} hexamers, 6-Aβ_{1-42} hexamers, 7-[E22G]Aβ_{1-40} hexamers, and 8-[E22G]Aβ_{1-42} hexamers.

Fig. S5: The average SASA per amino acid for (a) dimers and (b) hexamers of Aβ_{1-40} (solid black curves), Aβ_{1-42} (solid red curves), [E22G]Aβ_{1-40} (dotted black curves), and [E22G]Aβ_{1-42} (dotted red curves). The error bars correspond to SEM.

Fig. S6: *Intra*molecular contact maps for (a-d) dimers and (e-h) hexamers of Aβ_{1-40} (a,e), Aβ_{1-42} (b,f), [E22G]Aβ_{1-40} (c,g), and [E22G]Aβ_{1-42} (d,h). The lower triangle contains the average number of contacts between two amino acids and the upper triangle contains the average number of hydrogen bonds for each pair of amino acids. The scale on the right shows the color mapping. The two types of maps have different scales, the scale on the left corresponds to the average number of contacts and the scale on the right corresponds to the average number of hydrogen bonds. The two thin diagonal lines are drawn through the diagonal elements of the two types of contact maps. The rectangular gray boxes with numbers mark regions of interest.

Fig. S7: *Inter*molecular contact maps for (a-d) dimers and (e-h) hexamers of Aβ_{1-40} (a,e), Aβ_{1-42} (b,f), [E22G]Aβ_{1-40} (c,g), and [E22G]Aβ_{1-42} (d,h). The lower triangle contains the average number of contacts between two amino acids and the upper triangle contains the average number of hydrogen bonds for each pair of amino acids. The scale on the right shows the color mapping. The two types of maps have different scales, the scale on the left corresponds to the average number of contacts and the scale on the right corresponds to the average number of hydrogen bonds. The two thin diagonal lines are drawn through the diagonal elements of the two types of contact maps. The rectangular gray boxes with numbers mark regions of interest.

Fig. S1

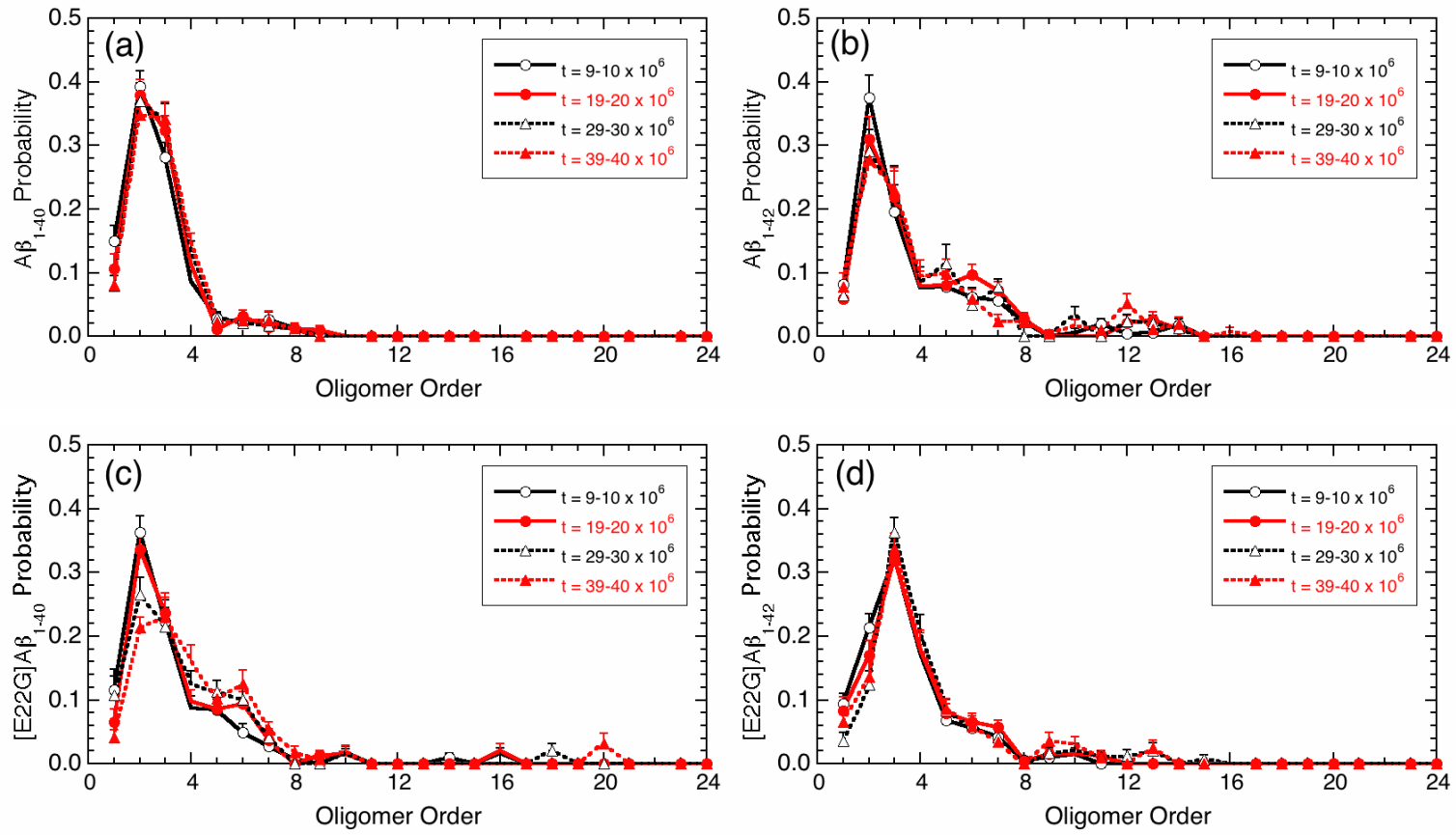
(a)
(b)
(c)
(d)
t = 9-10 x 10^6
t = 19-20 x 10^6
t = 29-30 x 10^6
t = 39-40 x 10^6
Aβ1-40 Probability
Aβ1-42 Probability
[E22G]Aβ1-40 Probability
[E22G]Aβ1-42 Probability
Oligomer Order
0.0
0.1
0.2
0.3
0.4
0.5
0
4
8
12
16
20
24

(a)

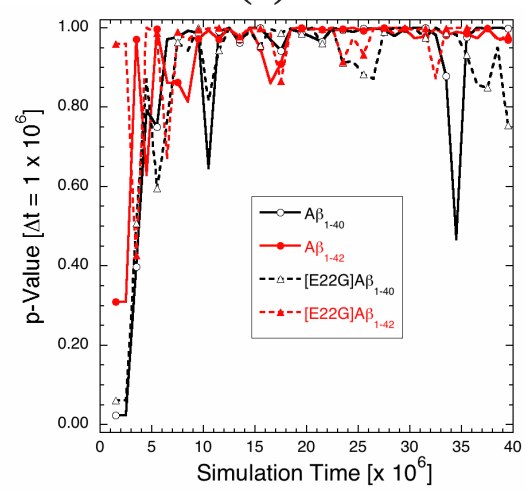
p-Value [Δt = 1 x 10^6]
Simulation Time [x 10^6]
Aβ1-40
Aβ1-42
[E22G]Aβ1-40
[E22G]Aβ1-42

(b)

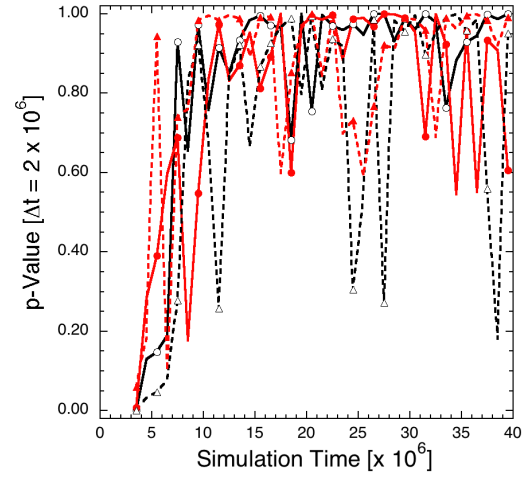
p-Value [Δt = 2 x 10^6]
Simulation Time [x 10^6]

(c)

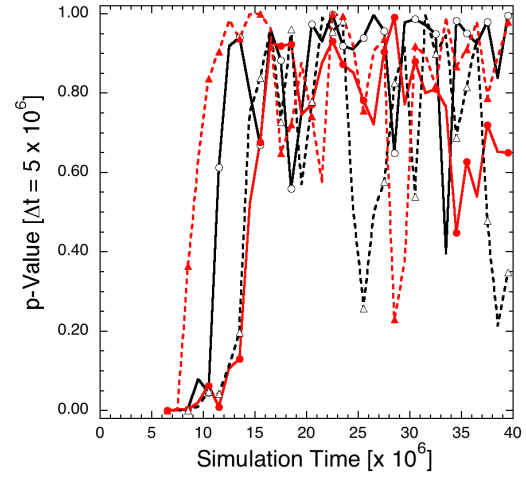
p-Value [Δt = 5 x 10^6]
Simulation Time [x 10^6]

Fig. S2

(a)

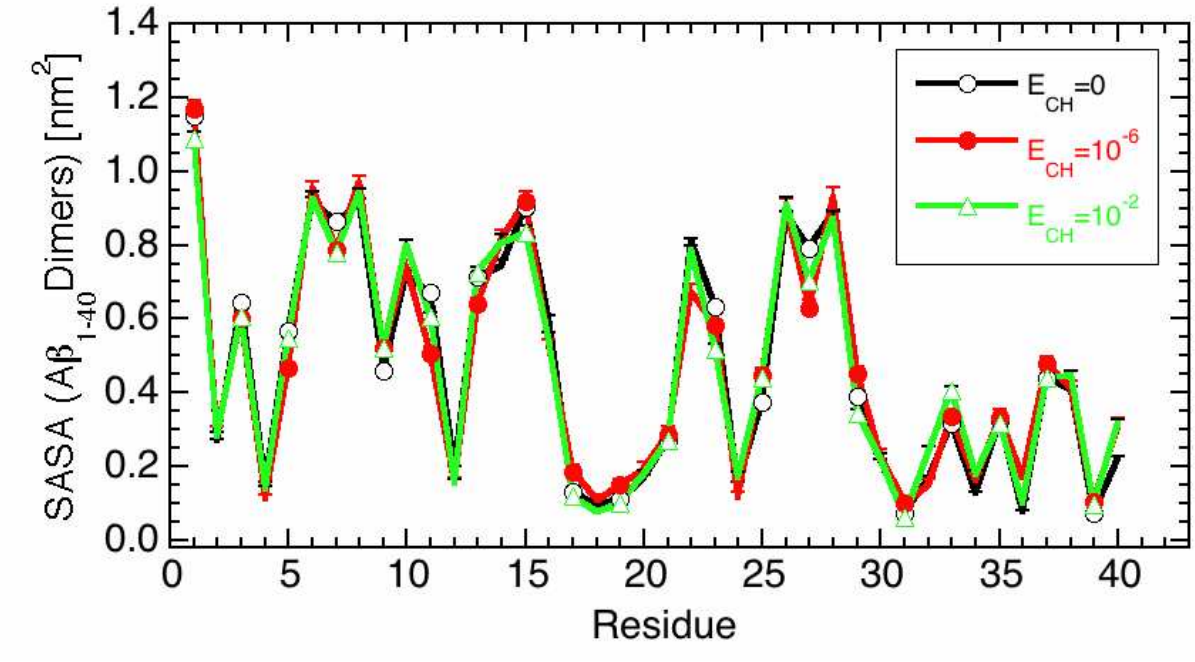
SASA (Aβ1-40 Dimers) [nm2]
Residue
ECH=0
ECH=10-6
ECH=10-2

(b)

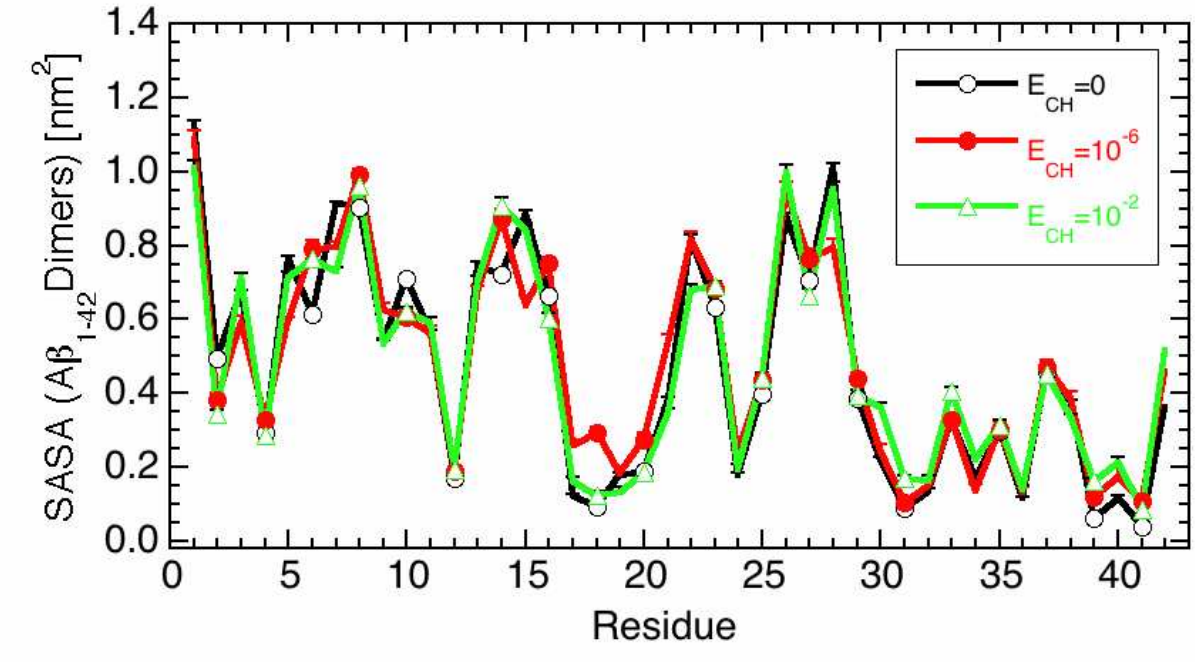
SASA (Aβ1-42 Dimers) [nm2]
Residue
ECH=0
ECH=10-6
ECH=10-2

Fig. S3

Fig. S4

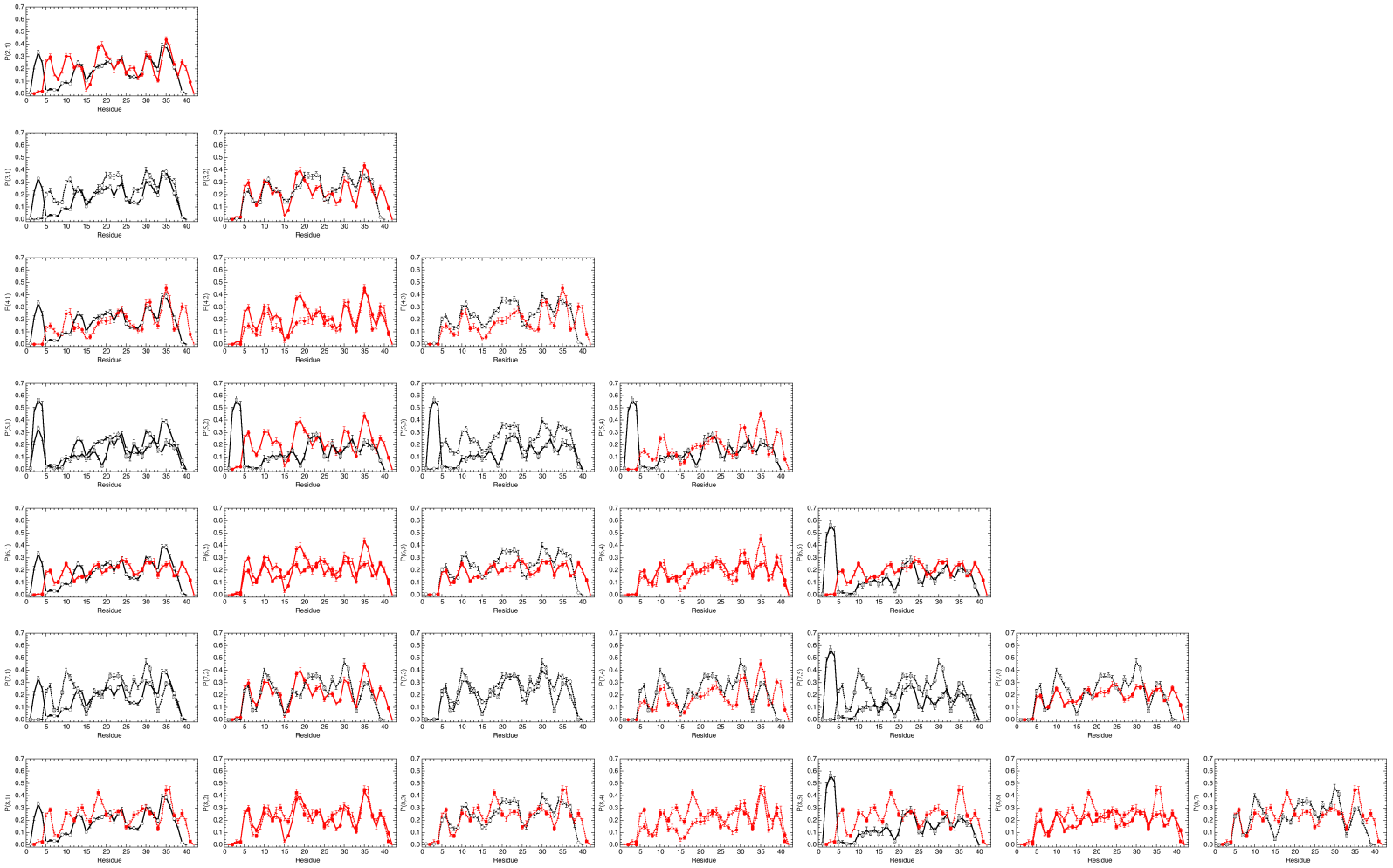
P(2,1)
P(3,1)
P(3,2)
P(4,1)
P(4,2)
P(4,3)
P(5,1)
P(5,2)
P(5,3)
P(5,4)
P(6,1)
P(6,2)
P(6,3)
P(6,4)
P(6,5)
P(7,1)
P(7,2)
P(7,3)
P(7,4)
P(7,5)
P(7,6)
P(8,1)
P(8,2)
P(8,3)
P(8,4)
P(8,5)
P(8,6)
P(8,7)
Residue

(a)

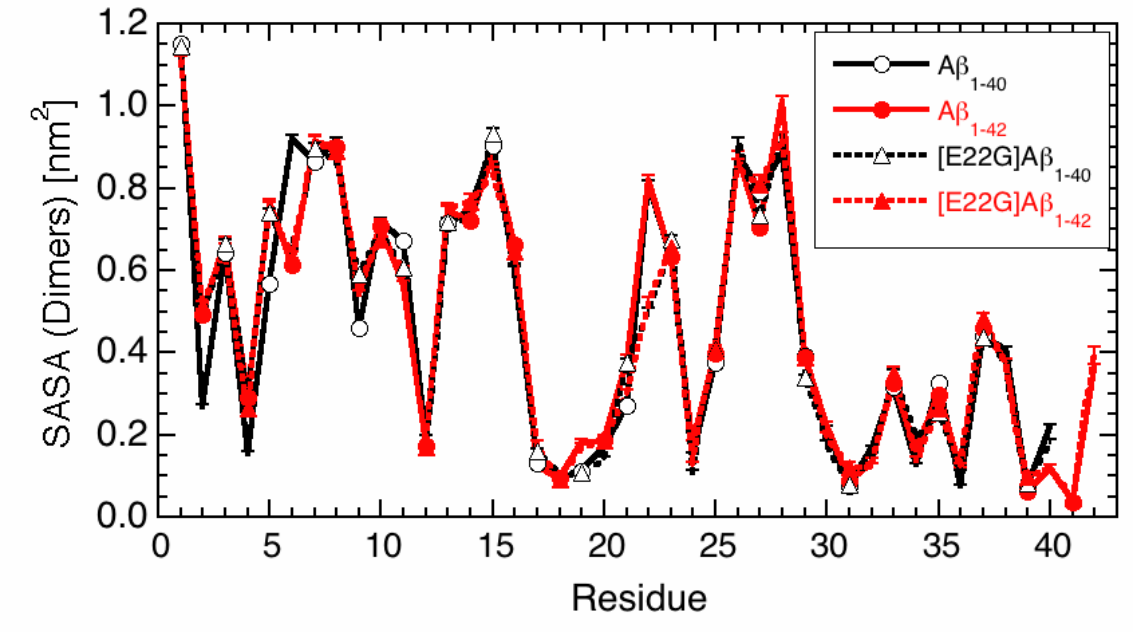
SASA (Dimers) [nm^2]
Residue
Aβ$_{1-40}$
Aβ$_{1-42}$
[E22G]Aβ$_{1-40}$
[E22G]Aβ$_{1-42}$

(b)

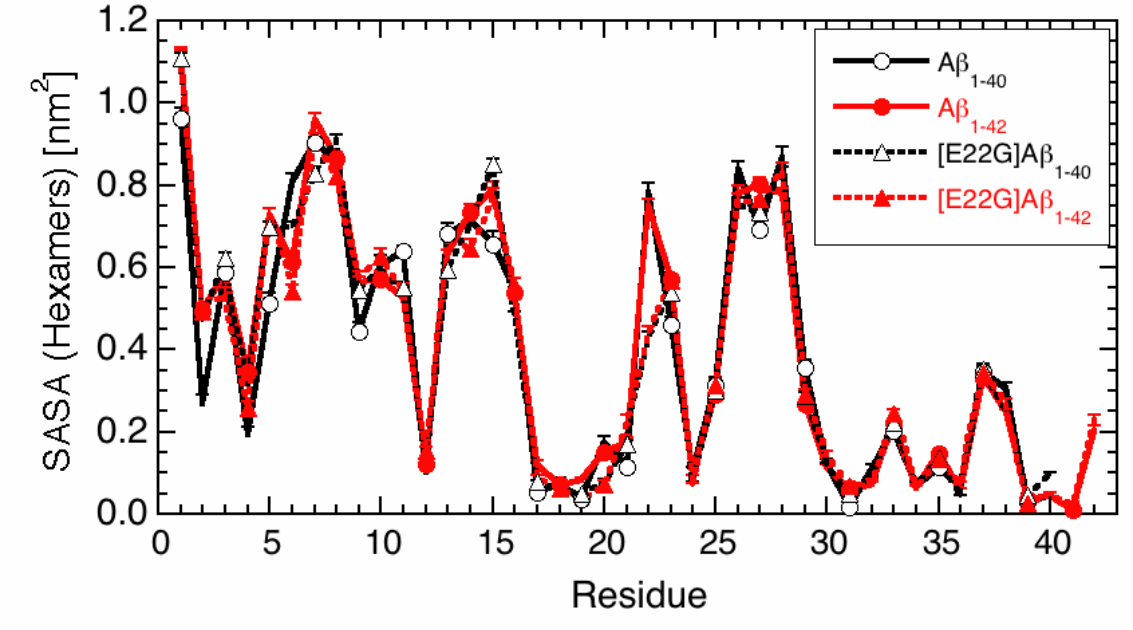
SASA (Hexamers) [nm^2]
Residue
Aβ$_{1-40}$
Aβ$_{1-42}$
[E22G]Aβ$_{1-40}$
[E22G]Aβ$_{1-42}$

Fig. S5

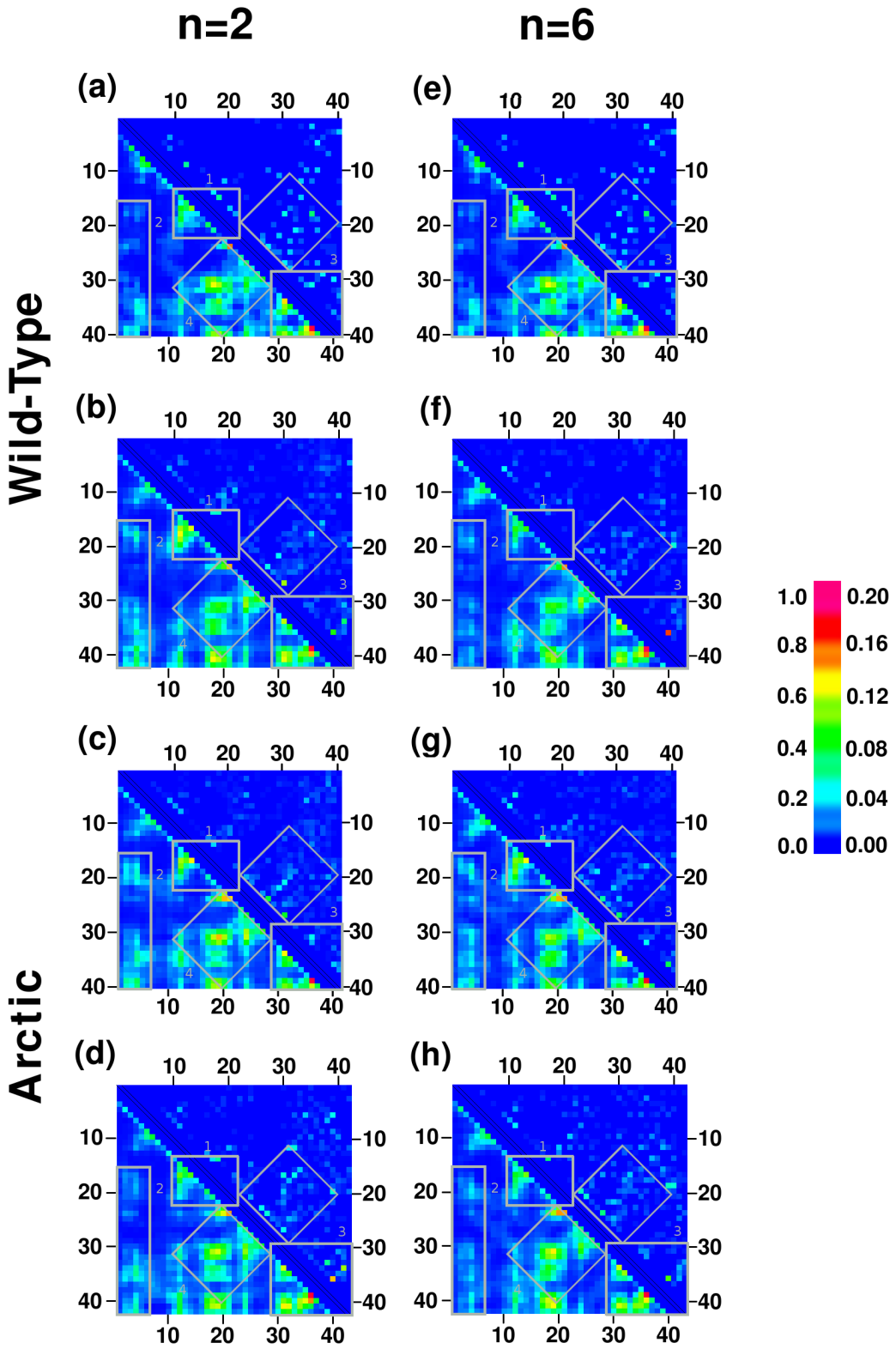
n=2
n=6
Wild-Type
Arctic
(a)
(b)
(c)
(d)
(e)
(f)
(g)
(h)
10
20
30
40
1
2
3
4
1.0
0.8
0.6
0.4
0.2
0.0
0.20
0.16
0.12
0.08
0.04
0.00

Fig. S6

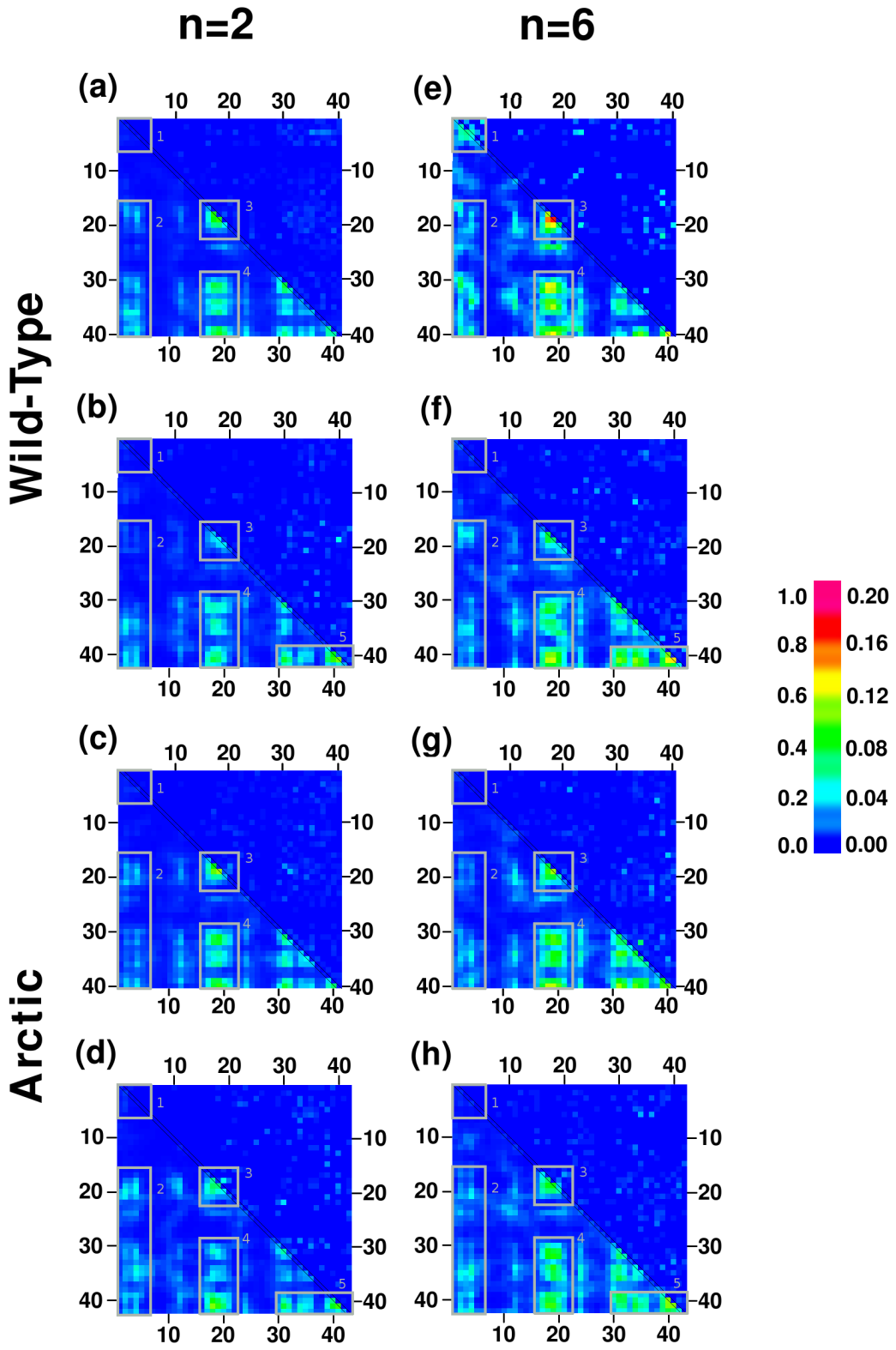
n=2
n=6
Wild-Type
Arctic
(a)
(b)
(c)
(d)
(e)
(f)
(g)
(h)
10
20
30
40
1
2
3
4
5
1.0
0.8
0.6
0.4
0.2
0.0
0.20
0.16
0.12
0.08
0.04
0.00

Fig. S7

(1) Bitan, G.; Vollers, S. S.; Teplow, D. B. *J. Biol. Chem.* **2003,** *278,* 34882–34889.

(2) Lam, A.; Teplow, D. B.; Stanley, H. E.; Urbanc, B. *J. Am. Chem. Soc.* **2008,** *130,* 17413-17422.

(3) Urbanc, B.; Cruz, L.; Yun, S.; Buldyrev, S. V.; Bitan, G.; Teplow, D. B.; Stanley, H. E. *Proc. Natl. Acad. Sci. USA.* **2004,** *101,* 17345–17350.

(4) Yun, S.; Urbanc, B.; Cruz, L.; Bitan, G.; Teplow, D. B.; Stanley, H. E. *Biophys J* **2007,** *92,* 4064-4077.